buildings

MDPI

Article

Study on the Vibration Comfort of a High-Rise Industrial Building

Xinxin Zhang [1], Ruoyang Zhou [2], Xiaoxiong Zha [2,*] and Yong Liao [1]

[1] China Construction Science and Industry Corporation Ltd., Shenzhen 518118, China; zhangxx2012@cscec.com (X.Z.); liaoyong2012@cscec.com (Y.L.)
[2] School of Civil and Environmental Engineering, Harbin Institute of Technology (Shenzhen), Shenzhen 518067, China; 20b354001@stu.hit.edu.cn
* Correspondence: zhaxx@hit.edu.cn

Abstract: This study assesses the vibration comfort of a steel–concrete composite floor system in a high-rise industrial building under construction in Shenzhen. The assessment focuses on human-induced vibrations. Acceleration time histories were recorded, and spectral analysis was conducted to identify the fundamental frequencies and damping ratios. A finite element model of the industrial building was developed to simulate the vibrational response under identical conditions. Additionally, vibration response calculations were carried out using standard methodologies. The performance of a Tuned Mass Damper (TMD) system was analyzed by comparing experimental, theoretical, and simulated results with standard thresholds. Prior to TMD installation, certain locations did not meet vibration comfort standards, but, following installation, all points were within acceptable limits. These findings demonstrate the TMD's effectiveness in enhancing vibration comfort.

Keywords: steel–concrete composite structure; vibration comfort; peak vibration acceleration; Tuned Mass Damper (TMD)

check for updates

Citation: Zhang, X.; Zhou, R.; Zha, X.; Liao, Y. Study on the Vibration Comfort of a High-Rise Industrial Building. *Buildings* **2024**, *14*, 3676. https://doi.org/10.3390/buildings14113676

Academic Editor: Eugeniusz Koda

Received: 31 October 2024
Revised: 15 November 2024
Accepted: 15 November 2024
Published: 19 November 2024

Copyright: © 2024 by the authors. Licensee MDPI, Basel, Switzerland. This article is an open access article distributed under the terms and conditions of the Creative Commons Attribution (CC BY) license (https://creativecommons.org/licenses/by/4.0/).

1. Introduction

The increasing height and complexity of high-rise industrial buildings present unique challenges in ensuring structural comfort, particularly in vibration-sensitive environments. While several studies have focused on the dynamic behavior of high-rise residential and office buildings, limited research has been conducted on industrial structures, which are often subjected to more severe operational and environmental loads. This study aims to fill this gap by evaluating the vibration comfort of a steel–concrete composite floor system in an under-construction high-rise industrial building in Shenzhen, emphasizing human-induced vibrations—a critical consideration in the design and operation of modern industrial facilities.

Human-induced vibrations are typically less predictable and more erratic compared to mechanical sources, necessitating sophisticated analysis and mitigation strategies to ensure occupant comfort and machinery precision. This research not only documents the vibrational characteristics of such a building through empirical measurements but also leverages advanced spectral analysis to delineate fundamental frequencies and damping ratios, essential for understanding the dynamic behavior of the structure.

Mello et al. (2008) introduced the moving load method based on human-induced load models to study the vibration of large-span floor systems, obtaining vibration responses through finite element analysis software [1]. Kim et al. (2008) utilized a multi-degree-of-freedom damping model of the human body to calculate the vibration response of large-span bridges subjected to the load of single and multiple individuals [2]. Silva et al. (2009) performed finite element simulations of large-span floors based on rhythmic crowd movement load models [3]. Song Zhigang [4] and Chen Yu [5] employed the moving pedestrian load method to calculate the acceleration response of large-span pedestrian

bridges, providing fitting expressions for the results. Chen Xin et al. (2010) used a multi-point input time history analysis method to calculate the vibration response of large-span floors under crowd loads [6]. Lou Yu's team (2012) investigated the vibration comfort of multi-story sports and fitness venue floor systems [7]. Li Quan et al. (2012) conducted research on large-span floors subjected to rhythmic crowd movements and proposed a random vibration model [8].

In 2014, Davis, Liu, and Murray proposed a simple and effective method for evaluating the comfort of low-frequency steel–concrete composite floors subjected to walking-induced vibrations [9]. Zhou Xuhong, Li Jiang, and Liu Jiepeng conducted finite element simulations and verifications in 2016, based on field drop tests of a prestressed concrete rigid-frame cable-stayed floor system [10]. In 2019, Liu Jiepeng, Zheng Xing, and Li Jiang performed single footfall and walking tests on precast concrete slabs with straight ribs, analyzing the peak acceleration and root mean square acceleration values [11].

A significant portion of this study involves the development and validation of a finite element model (FEM) that simulates the vibrational response under identical conditions to those recorded in situ. This model is instrumental in verifying theoretical predictions against actual performance, thus providing a robust framework for evaluating different vibration mitigation techniques.

Furthermore, this research assesses the efficacy of a Tuned Mass Damper (TMD) system, a critical component in passive vibration control strategies. A Tuned Mass Damper (TMD) is a passive control device that can effectively mitigate micro-vibrations induced by the traffic environment. The operational mechanism of a TMD is such that, when a structure is excited by external forces and begins to vibrate, it concurrently activates the TMD system. The relative motion of the TMD system generates inertial forces that act back on the structure, thereby reducing the structural vibration response.

Studies have explored multi-degree-of-freedom TMDs and Multiple Tuned Mass Damper (MTMD) systems, which provide enhanced vibration control by targeting several resonant frequencies simultaneously. Such systems have shown promising results in high-rise applications, where varied dynamic modes may require a broader damping effect [12]. Additionally, semi-active and hybrid TMD designs have gained attention, integrating passive TMDs with active control elements to adapt to changing load conditions in real time, thereby improving efficiency in environments with variable external forces [13].

By integrating experimental, theoretical, and simulated data, the study not only demonstrates the TMD's effectiveness but also benchmarks its performance against standard thresholds. Prior to the installation of the TMD, certain locations within the building did not meet the vibration comfort standards. However, post-installation, all measured points fell within acceptable limits, showcasing the TMD's role in enhancing occupant comfort and operational stability.

Through this work, we aim to contribute uniquely to the field by providing detailed insights into the dynamic responses of high-rise industrial buildings to human-induced vibrations and demonstrating the practical application and benefits of TMD systems in such contexts. This study not only advances our understanding of structural dynamics in industrial settings but also offers a methodological blueprint for future research in this critical area of civil engineering.

2. Model Overview

The project features a steel–concrete composite frame structure. The large-span area is shown within the framed region of Structural Plan in Figure 1. The beams are constructed from Q355B steel, with section dimensions provided in Table 1. The columns consist of concrete-filled steel tubes, also utilizing Q355B steel. The concrete with a strength grade of C60 is used within the steel tubes, the steel tube thickness is 10 mm, and the column diameter is 600 mm. The floor system is built using a steel rebar truss deck, with the floor concrete having a strength grade of C30 and a thickness of 150 mm.

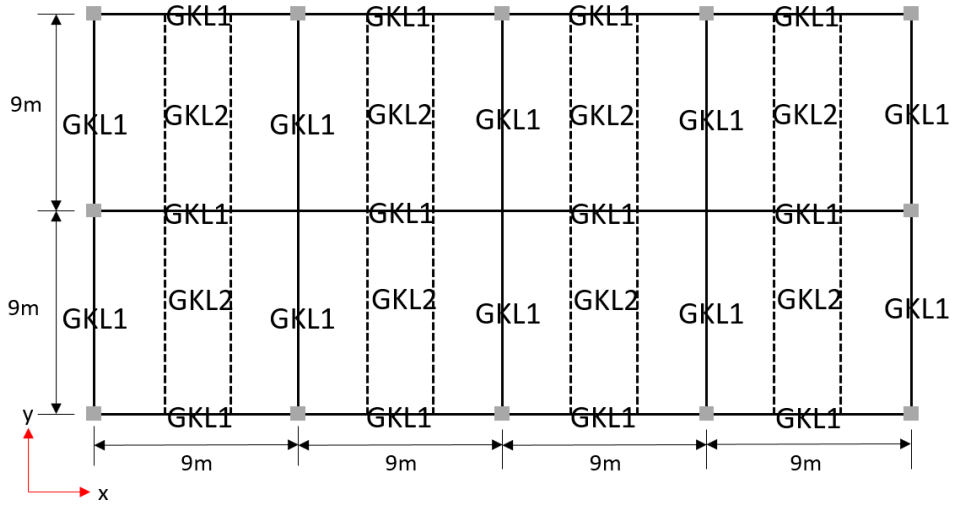


Figure 1. Structural plan of an industrial buildings.

Table 1. Dimensions of beam.

Part Number	$H \times B \times T_f \times T_w$	Steel Designation
GKL1	H1000 × 400 × 20 × 38	Q345B
GKL2	H900 × 200 × 15 × 26	Q355B

The limitations are derived from the "Technical Standards for Vibration Comfort of Building Floors (JGJ/T 441-2019)" [14], which outline the requirements for sports venues: "For floor structures primarily subjected to rhythmic activities, the first-order natural frequency in the vertical direction should not be less than 4 Hz, and the peak vertical acceleration must remain within the specified limits", as outlined in Table 2.

Table 2. Limit value for peak vertical vibration acceleration.

Part Number	Peak Acceleration ($m \cdot s^{-2}$)
Workshop office	0.20
Production operation area	0.40

3. Vibration Testing of the Sports Field Floor

3.1. Testing Background

To mitigate potential vibration comfort issues, comprehensive on-site tests were performed under various conditions on the composite floor of the industrial buildings. If the vibration comfort did not meet regulatory standards, the installation of Tuned Mass Dampers (TMDs) was planned as a remedial measure. Real-life images are provided in Figure 2.

The testing was conducted at an active construction site where work proceeded continuously on weekdays, except during a lunch break from 12:00 P.M. to 2:00 P.M. Due to the potential presence of various high-frequency noise interferences at the construction site, measures were taken to ensure data quality. Specifically, a low-pass filter with a cutoff frequency of 5 Hz was configured on the signal acquisition equipment to mitigate interference from construction-related signals. Additionally, the testing period was selected to occur between 12:00 P.M. and 2:00 P.M. to avoid active construction times and further reduce noise interference. To account for environmental noise, the signal acquisition equipment was also equipped with an automatic environmental signal processing function; by enabling this function, the device could intelligently filter out environmental signals during data collection.



Figure 2. Real-life image of an industrial buildings.

3.2. Test Plan

3.2.1. Test Content

Nine measurement points were established at the mid-span of the floor slab. The stimuli were applied along the direction of y, also at the mid-span of the floor slab. The arrangement of the measurement points and the stimulus path are illustrated in Figure 3.

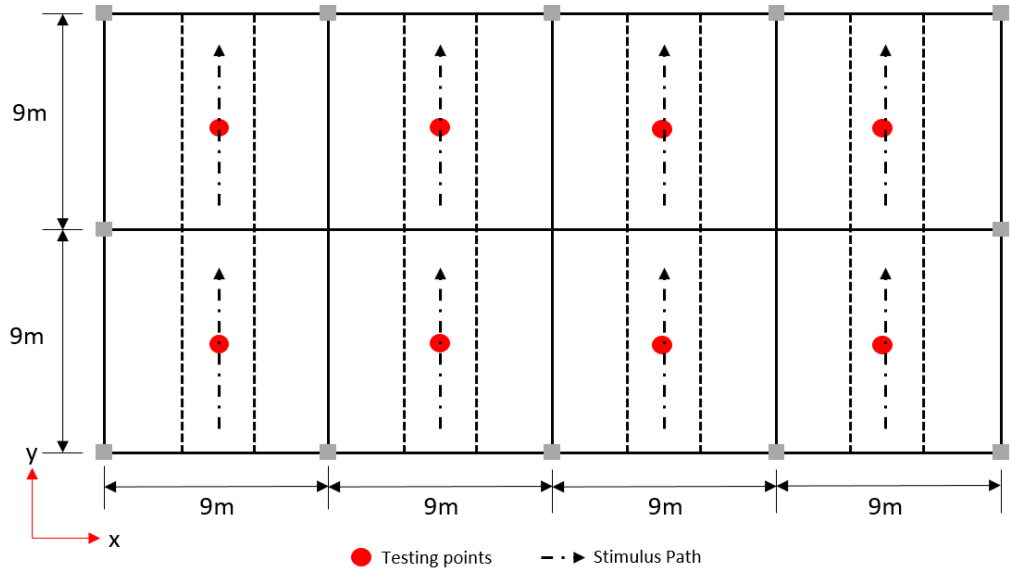


Figure 3. Schematic diagram of measurement points and excitation path.

Jumping Condition: A tester weighing 80 kg was used. Before initiating the test, the tester remained stationary at the designated test point, with knees bent at a 90-degree angle. Upon commencement, the tester jumped and then naturally landed, ensuring body stability throughout the process. Data collection continued until the recorded data returned to a stable state.

Walking Condition: A tester weighing 80 kg walked steadily along the stimulus path at a pace of 1 m/s, with a step frequency of 2 Hz.

Running Condition: A tester weighing 80 kg ran along the stimulus path at a consistent speed of 2 m/s, with a step frequency of 2 Hz.

The movement frequency for the above test conditions was controlled using a metronome app downloaded on a smartphone. The app was set to the desired beat intervals, such as

one beat per second, enabling testers to synchronize their jumps, walking, or running with the beat, thus achieving a movement frequency of 1 Hz.

For controlling the pace during walking and running, the following tests were carried out:

Walking Test: Control points were placed at 0.5 m intervals along the stimulus path. The metronome was set to beat twice per second, and testers moved to the next control point with each beat, maintaining a step frequency of 2 Hz and a walking pace of 1 m/s.

Running Test: Control points were spaced 1 m apart along the stimulus path. Similarly, the metronome was set to beat twice per second, and testers ran to the next control point at each beat, achieving a step frequency of 2 Hz and a running pace of 2 m/s.

The test conditions are shown in Table 3.

Table 3. Test Conditions.

	Body Weight/kg	Step Speed/(m/s)	Step Frequency/Hz	Control Point Spacing/m
Jump	80			
Walk	80	1	2	0.5
Run	80	2	2	1

3.2.2. Test Equipment

(1) The Donghua 1A401E sensor was used to collect acceleration time–history curves at the measurement points. The sensitivity setting of the sensor was set to 5.183 V/(m·s^{-2}). This setup is illustrated in Figure 4.



Figure 4. Donghua 1A401E sensor.

(2) The Donghua DH8303 dynamic signal test analyzer was used for data collection. The analyzer was used in combination with the DHDAS dynamic signal acquisition and analysis software. The sampling frequency was set to 1000 Hz. This system enabled the direct conversion and calculation of charge signals captured by the sensor. It allowed for the output of acceleration data to the PC. This setup is shown in Figure 5.



Figure 5. Donghua DH8303 dynamic signal test analyzer.

3.2.3. Equipment Selection Description

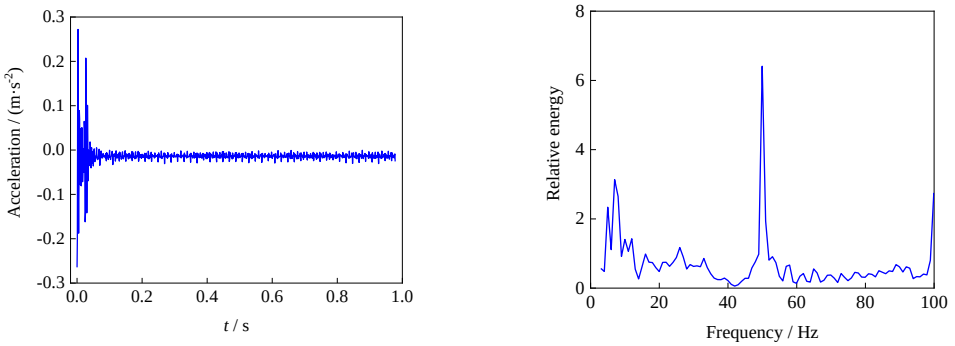
Donghua 1A401E designed with high-sensitivity piezoelectric ceramics are selected for its good signal-to-noise ratio and high measurement resolution. Lightweight materials, such as titanium alloy or aluminum alloy, are used for the casing to reduce the added mass on the measured object and improve the accuracy of the test data.

The DH8303N Dynamic Signal Testing and Analysis System is specifically designed for analyzing the dynamic characteristics of structures, with each channel equipped with an independent 32-bit A/D converter. It adopts a 19-inch standard chassis structure and utilizes a gigabit Ethernet switch for expansion, allowing a single computer to perform the parallel, synchronized testing and analysis of an unlimited number of vibration signal channels.

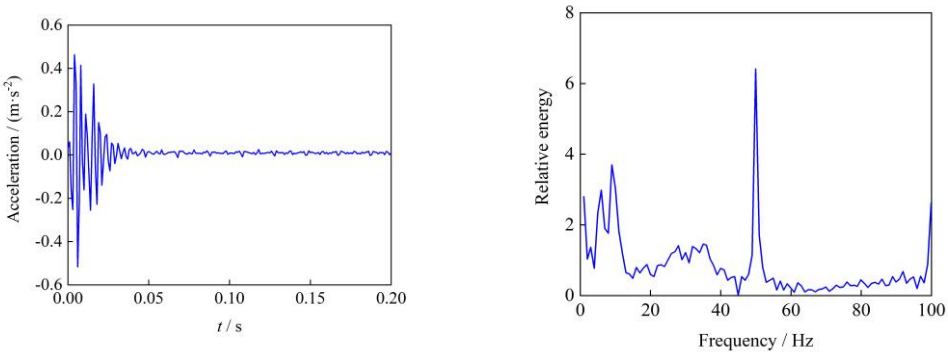
3.3. Testing Result

3.3.1. Vertical Natural Frequency Test

The resulting acceleration time–history curves of the floor's vertical vibration, along with the corresponding spectral curves obtained via FFT transformation, are shown in Figure 6. The first-order natural frequencies in the vertical direction are summarized in Table 4. Given the low frequency of the jumping excitation load, a low-pass filter was applied to smooth the curves, allowing only low-frequency signals to pass while filtering out irrelevant interference. The cutoff frequency was set at 5 Hz.

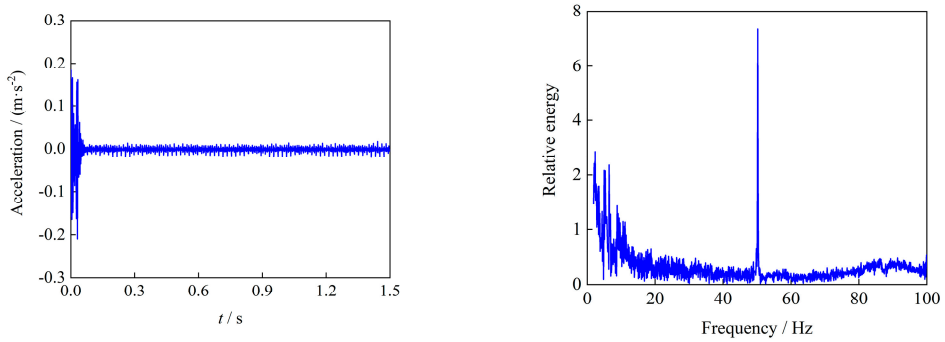


(**a**) Test Point 1

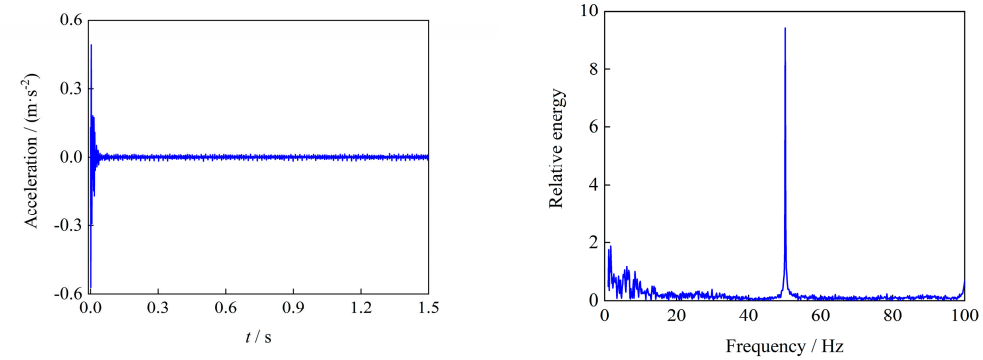


(**b**) Test Point 2

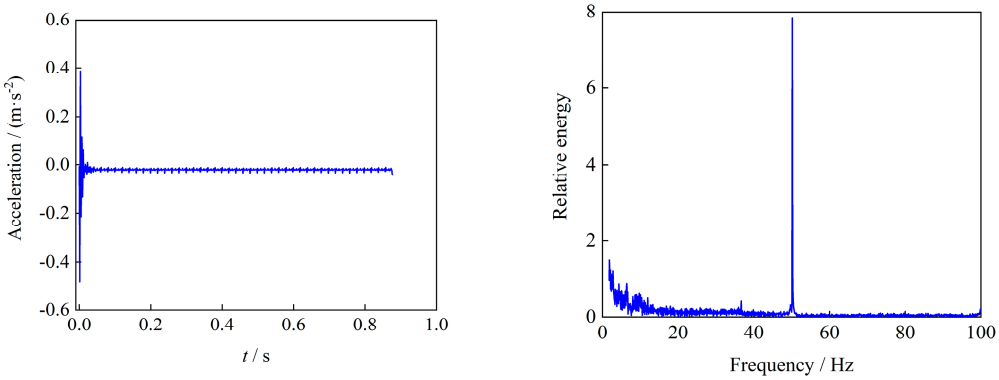
Figure 6. *Cont.*



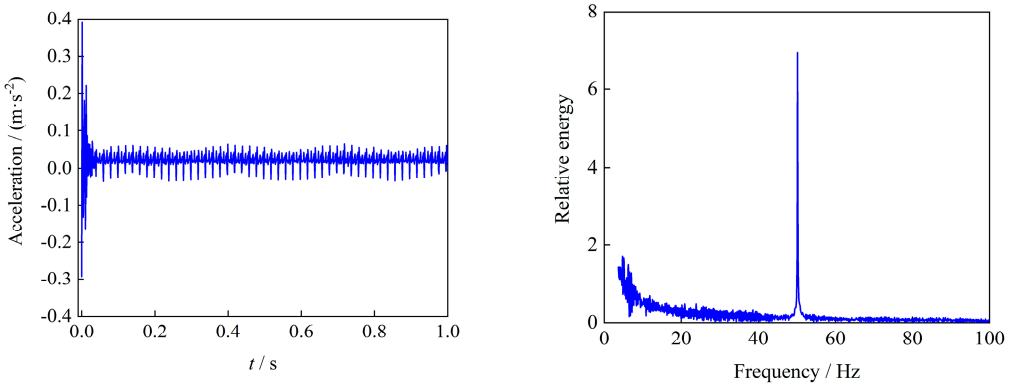
(**c**) Test Point 3



(**d**) Test Point 4

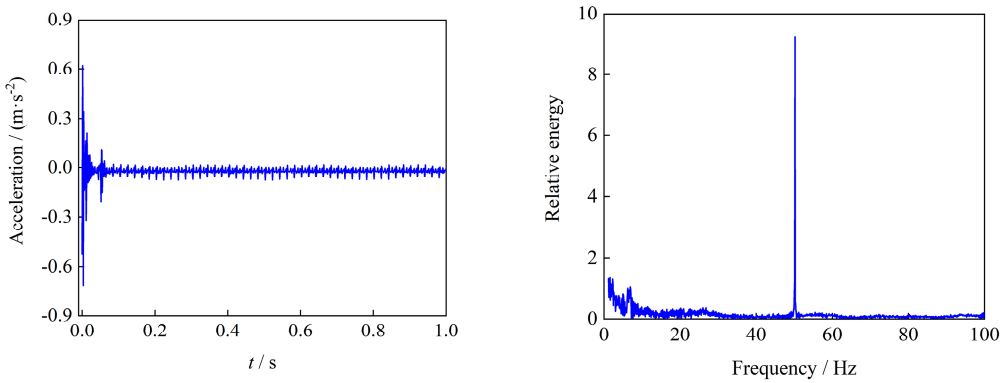


(**e**) Test Point 5

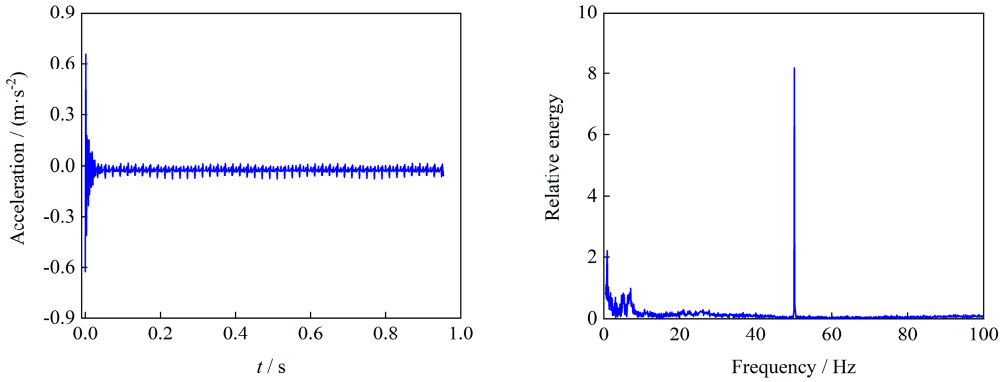


(**f**) Test Point 6

Figure 6. *Cont.*



(**g**) Test Point 7



(**h**) Test Point 8

Figure 6. Vertical vibration acceleration of floor slab under jump excitation and spectrum curve conversion.

Table 4. First−order vertical natural frequency.

Floor	*f*/Hz
Point 1	4.99
Point 2	4.99
Point 3	5.31
Point 4	5.14
Point 5	5.19
Point 6	5.21
Point 7	5.30
Point 8	5.23

In the course of our analysis, we meticulously extracted the first−order vertical natural frequencies of the floor slabs for each individual floor. This crucial data, pivotal for understanding the dynamic behavior of the building's floors, has been comprehensively tabulated. For a detailed overview of these natural frequencies, readers are directed to consult Table 4. This table provides an organized and accessible presentation of the extracted frequencies, thereby facilitating a clear understanding of the vibrational characteristics across different levels of the building.

As shown in Table 4, according to Technical Standards for Vibration Comfort of Building Floors (JGJ/T 441-2019), the vertical natural frequencies measured at all measurement points exceed the 4 Hz threshold specified by the standards, ensuring compliance with vibration comfort requirements.

3.3.2. Damping Ratio

The half-power bandwidth method is used to calculate the damping ratio, where f_2 represents the frequency at 0.707 times the peak resonance value on the left side, f_1 represents the frequency at 0.707 times the peak resonance value on the right side, f_0 is the peak resonance frequency, and ξ is the damping ratio.

The damping ratio of the tested floor slab was calculated. The results of these calculations are summarized in Table 5.

Table 5. Calculated damping ratio of the floor slab.

Measurement Points	f_2	f_1	f_0	ξ
Point 1	5.51	4.68	4.99	0.083
Point 2	5.49	4.69	4.99	0.080
Point 3	5.55	4.68	5.30	0.082
Point 4	5.47	4.66	5.14	0.079
Point 5	5.59	4.7	5.19	0.086
Point 6	5.60	4.75	5.20	0.082
Point 7	5.44	4.62	5.30	0.077
Point 8	5.64	4.78	5.23	0.082

As shown in Table 5, the calculated damping ratios for the floor slab are approximately 0.08. Therefore, in the subsequent theoretical calculations and finite element modeling, a damping ratio of 0.08 is adopted for the floor slab.

3.3.3. Vertical Peak Acceleration Test

The acceleration Time-history curves for the floor slab's vertical vibration are presented in Figure 7. The vertical peak accelerations obtained from these tests are summarized in Table 6. Given the low frequency of human-induced loads in each condition, a low-pass filter was applied to smooth the curves, allowing only low-frequency signals to pass and eliminating interference from unrelated signals. The cutoff frequency was set to 5 Hz.

For Point 1, under walking conditions at a 95% confidence level, the confidence interval for the mean acceleration is approximately [0.0036, 0.0046] $m{\cdot}s^{-2}$; under running conditions at a 95% confidence level, the confidence interval for the mean acceleration is approximately [0.0012, 0.0023] $m{\cdot}s^{-2}$.

For Point 2, under walking conditions at a 95% confidence level, the confidence interval for the mean acceleration is approximately [0.0022, 0.0031] $m{\cdot}s^{-2}$; under running conditions at a 95% confidence level, the confidence interval for the mean acceleration is approximately [0.0032, 0.0036] $m{\cdot}s^{-2}$.

For Point 3, under walking conditions at a 95% confidence level, the confidence interval for the mean acceleration is approximately [0.0025, 0.0035] $m{\cdot}s^{-2}$; under running conditions at a 95% confidence level, the confidence interval for the mean acceleration is approximately [0.0011, 0.0034] $m{\cdot}s^{-2}$.

For Point 4, under walking conditions at a 95% confidence level, the confidence interval for the mean acceleration is approximately [0.0012, 0.0025] $m{\cdot}s^{-2}$; under running conditions at a 95% confidence level, the confidence interval for the mean acceleration is approximately [0.0021, 0.0032] $m{\cdot}s^{-2}$.

For Point 5, under walking conditions at a 95% confidence level, the confidence interval for the mean acceleration is approximately [0.0018, 0.0024] $m{\cdot}s^{-2}$; under running conditions at a 95% confidence level, the confidence interval for the mean acceleration is approximately [0.0025, 0.0029] $m{\cdot}s^{-2}$.

For Point 6, under walking conditions at a 95% confidence level, the confidence interval for the mean acceleration is approximately [0.0024, 0.0034] $m{\cdot}s^{-2}$; under running conditions at a 95% confidence level, the confidence interval for the mean acceleration is approximately [0.0015, 0.0028] $m{\cdot}s^{-2}$.

For Point 7, under walking conditions at a 95% confidence level, the confidence interval for the mean acceleration is approximately [0.0034, 0.0042] $m{\cdot}s^{-2}$; under running

conditions at a 95% confidence level, the confidence interval for the mean acceleration is approximately [0.0035, 0.0041] $m \cdot s^{-2}$.

For Point 8, under walking conditions at a 95% confidence level, the confidence interval for the mean acceleration is approximately [0.0028, 0.0042] $m \cdot s^{-2}$; under running conditions at a 95% confidence level, the confidence interval for the mean acceleration is approximately [0.0025, 0.0031] $m \cdot s^{-2}$.

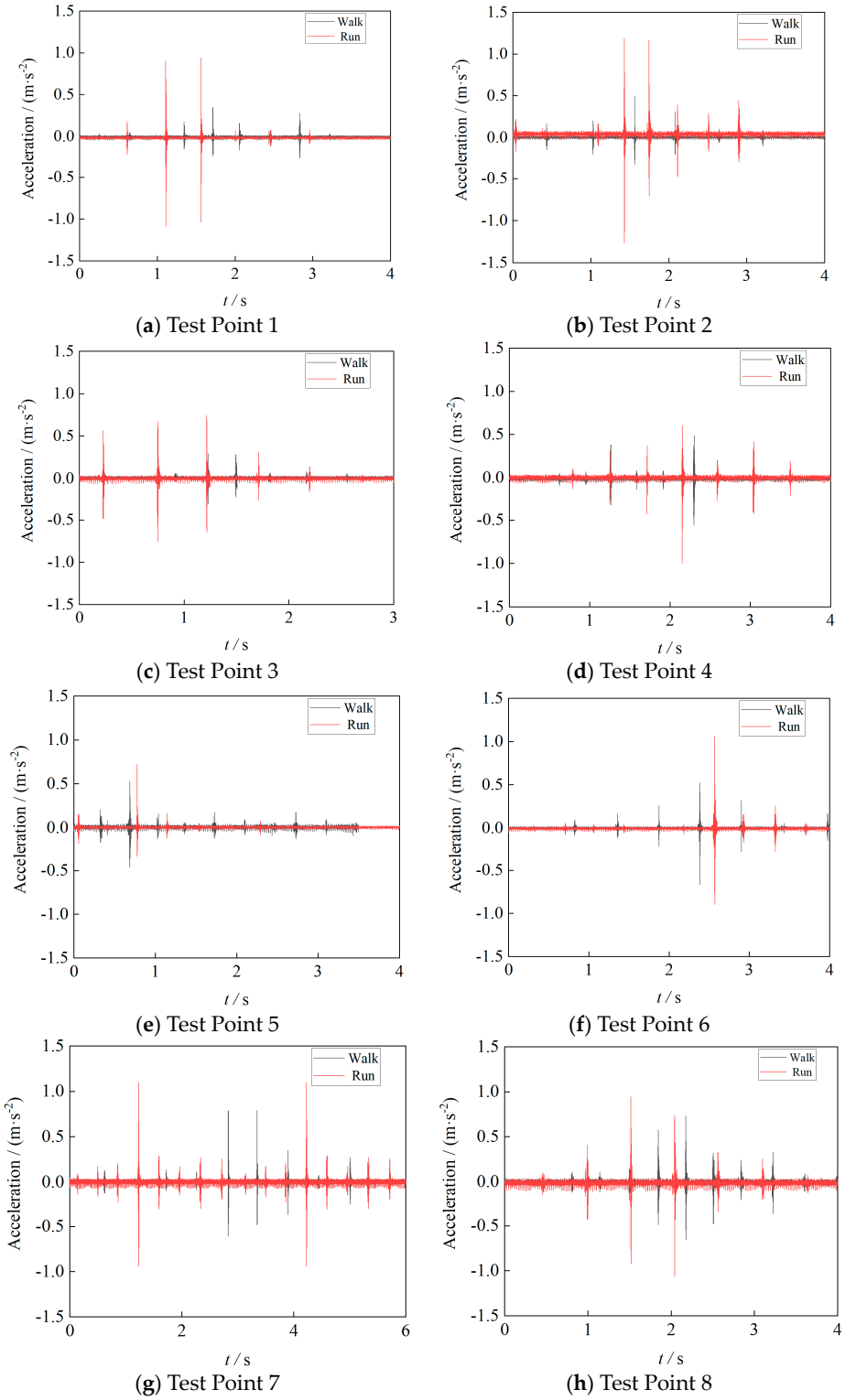


Figure 7. Time-history curves of floor vertical vibration acceleration.

Table 6. Test result of peak vertical vibration acceleration.

Measurement Points	Peak Acceleration/m·s^{-2}	
	Walk	Run
Point 1	0.346	1.089
Point 2	0.493	1.265
Point 3	0.307	0.753
Point 4	0.560	0.998
Point 5	0.529	0.720
Point 6	0.666	1.056
Point 7	0.788	1.099
Point 8	0.731	1.063

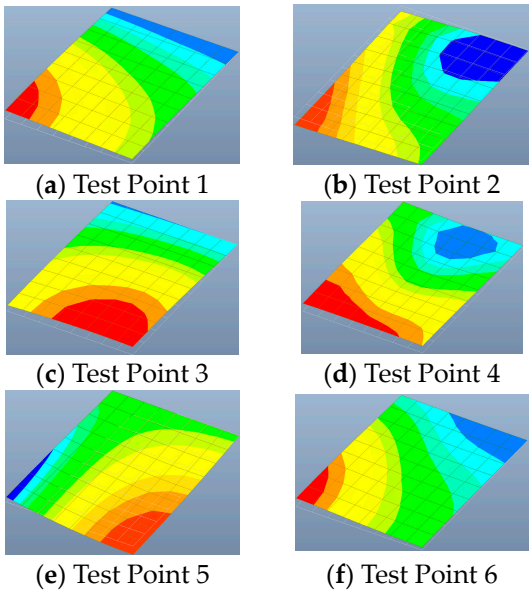
To validate the accuracy of the test results, the peak acceleration of floor vibrations induced by walking can be approximated using the following formula, as specified in the "Technical Standards for Vibration Comfort of Building Floors (JGJ/T 441-2019)":

$$\alpha_p = \frac{F_p}{\xi W} g$$
$$F_p = P_0 e^{-\beta}$$

where,

$$W = \frac{\Delta_j W_j + \Delta_g W_g}{\Delta_j + \Delta_g}; W_j = \delta F_{jk} B_{Ej} L_j$$
$$W_g = \delta F_{gk} B_{Eg} L_g; B_{Ej} = C_j \left(\frac{D_s}{\frac{I_j}{S_j}}\right)^{0.25} L_j$$
$$B_{Eg} = C_g \left(\frac{\frac{I_j}{S_j}}{\frac{I_g}{L_j}}\right)^{0.25} L_g;\ D_s = \frac{h_0^3 E_c}{8.89 E_s}$$
$$P_0 = R\sqrt{W}, R\ is\ reduction\ factor; \beta\ = 0.35 f_1$$

As shown in Figure 8 and Table 7, all measurement points exceeded the specified limit of 0.4 m/s^2 under at least one condition. According to Table 6, the theoretical peak acceleration calculations closely align with the test results, and conform to vibration comfort standards" for conciseness.

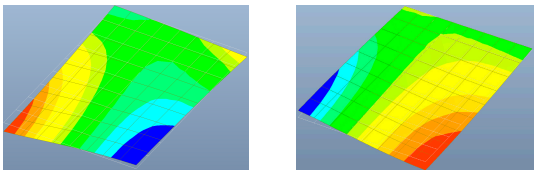


(**a**) Test Point 1 (**b**) Test Point 2

(**c**) Test Point 3 (**d**) Test Point 4

(**e**) Test Point 5 (**f**) Test Point 6

Figure 8. *Cont.*



(**g**) Test Point 7 (**h**) Test Point 8

Figure 8. Simulated floor vertical mode shape diagram.

Table 7. Theoretical peak vibration acceleration under walking load.

Measurement Points	f/Hz	F_P/kN	ξ	W/kN	Peak Acceleration/m·s^{-2}	
					Theory	Test
Point 7	5.30	0.454	0.077	81	0.713	0.788
Point 8	5.23	0.465	0.082	81	0.686	0.731

4. Finite Element Simulation of the Sports Field Floor

The finite element software used in this study is MADIS GEN 2021(v3.1), where beam and column elements are modeled using line elements, and slabs are modeled using shell elements. The boundary condition at the beam–slab connection is considered as fixed, while the boundary condition at the slab–column connection is set as rigid. According to the *Technical Standards for Vibration Comfort of Building Floors (JGJ/T 441-2019)*, in large-scale data experiments using finite element simulation, the recommendation is to increase the elastic modulus of materials by a factor of 1.2 to better simulate the real performance of the materials. The material damping was defined using the "strain energy factor", and the damping ratio was determined based on the values calculated in Table 5. The load application process was conducted as follows: First, the "Static Load" module was used to apply the live load at the designated target point. Next, in the "Seismic Action" module, a load case was defined with the analysis type set to "linear" and the analysis method selected as the "mode superposition method". After that, in the "Time History Function" module, a harmonic function matching the frequency and amplitude used in the experiment was added. Finally, in the "Time-Dependent Static Load" module, the previously defined static load was converted into a dynamic load, thus completing the load setup.

To obtain the finite element analysis results, the target points were grouped in advance. Once the computation was completed, the results for the points within this group could be directly extracted.

To account for dynamic effects, the material's elastic modulus was modified by applying an expansion coefficient of 1.2, reflecting the material's behavior under dynamic loading conditions. The rigidity of the inter-floor slabs was excluded from the model, and any stiffness constraints related to these slabs were removed.

4.1. Vertical Natural Frequency Simulation

The simulation results for the vertical vibration mode of the overall structure, as well as the vertical vibration mode of the composite floor slab in the test area, are shown in Figure 8.

The modal data for the floor slab at Test Point 1 have been extracted and are presented in Table 8. The data indicate that the vertical participation mass is highest in the sixth mode, signifying that this mode is the structure's first vertical mode. Modal analysis at Test Point 1 identified a vertical natural frequency of 5.02 Hz, as shown in Table 9.

Using the same methodology, the vertical natural frequencies for the other measurement points were extracted, and a summary of the frequencies for all measurement points is provided in Table 10. A comparison of the simulation and test results reveals minimal discrepancies, confirming the accuracy of the finite element model.

Table 8. Participation mass of mode shape at Measurement Point 1 on the floor slab.

Mode Number	Mode Participation Quality					
	TRAN-X		TRAN-Y		TRAN-Z	
	Mass (%)	Sum (%)	Mass (%)	Sum (%)	Mass/%	Sum (%)
1	70.73	70.73	6.78	6.78	0.18	0.18
2	2.43	73.16	90.83	97.61	0.01	0.19
3	0.50	73.66	0.27	97.88	0.00	0.19
4	23.33	96.99	0.55	98.43	0.24	0.43
5	0.87	97.86	0.72	99.15	0.00	0.43
6	0.23	98.09	0.28	99.43	7.90	8.33
7	0.19	98.28	0.00	99.43	1.21	9.54
8	0.25	98.53	0.11	99.54	0.01	9.55
9	0.04	98.57	0.14	99.68	0.01	9.56
10	0.13	98.7	0.18	99.86	0.00	9.56

Table 9. Modal analysis data for Measurement Point 1 on the floor slab.

Mode Number	Frequency (Hz)	
	(rad/s)	(cycle/s)
1	27.08053	4.31
2	29.15398	4.64
3	29.53097	4.70
4	30.59911	4.87
5	31.10177	4.95
6	31.54159	5.02
7	32.23274	5.13
8	32.60973	5.19
9	33.04955	5.26
10	33.48938	5.33

Table 10. First vertical natural frequency.

Measurement Points	Frequency (Hz)		Error (%)
	Test	Simulation	
1	4.99	5.02	0.60
2	4.99	5.01	0.40
3	5.30	5.09	4.18
4	5.14	5.08	1.20
5	5.19	5.06	2.59
6	5.20	5.05	2.99
7	5.30	5.02	5.58
8	5.16	5.01	2.99

In general, testing conditions are complex and uncontrollable, whereas finite element simulations are relatively stable. The frequency results from testing are derived from the FFT method applied to the acceleration time–history curve. Even for the same point, the FFT results will not be exactly the same each time but will be close to a reference point. Therefore, the test frequency and simulation frequency cannot be entirely identical. However, when comparing the results of the eight measurement points with the simulation, the average error is only 2.99%, which is quite small, indicating that the results are reliable.

4.2. Peak Vertical Acceleration Simulation

For the simulation of vertical peak acceleration, the human-induced loads were applied along the same paths and with the same magnitudes as those used in the experimental phase. The load time–history function was based on the classical Bachmann model for human-induced loads, ensuring that the simulation load cases precisely mirrored the test

conditions. The acceleration time–history curves for the floor slab vibration in the test area were extracted and are shown in Figure 9.

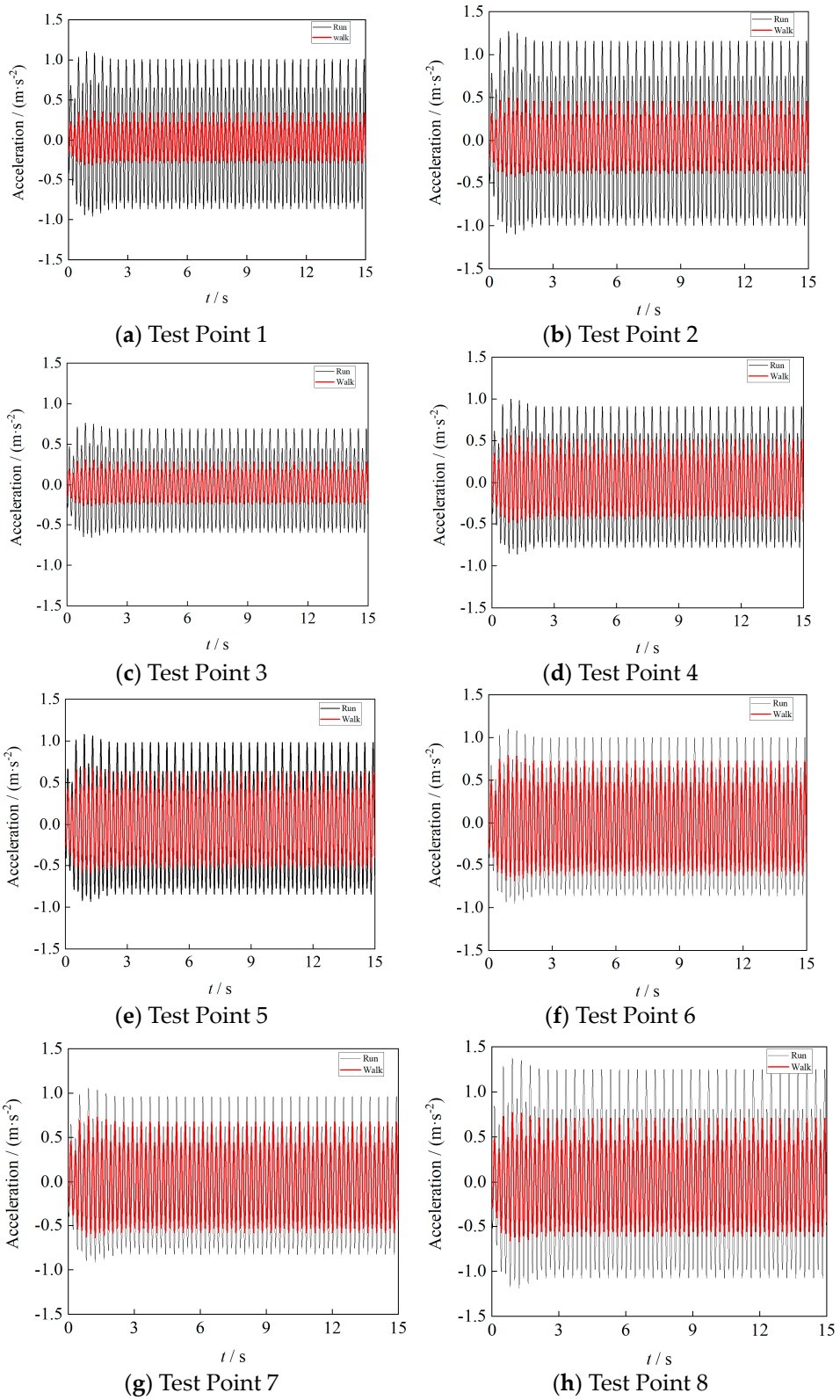


Figure 9. Simulation result of time-history curve of vibration acceleration.

The simulated peak vibration accelerations are summarized in Table 11, showing that the discrepancy between the simulation and test results is within 5%. This small margin of error effectively confirms the accuracy of the finite element model.

Table 11. Test and simulation result of peak vertical vibration acceleration.

Measurement Points	Peak Acceleration ($m \cdot s^{-2}$)					
	Walk			Run		
	Test	Simulation	Error (%)	Test	Simulation	Error (%)
Point 1	0.346	0.366	5.46	1.089	1.094	0.46
Point 2	0.493	0.494	0.20	1.265	1.273	0.63
Point 3	0.307	0.307	0	0.753	0.764	1.44
Point 4	0.560	0.561	0.18	0.998	1.00	0.2
Point 5	0.529	0.527	0.38	0.720	0.720	0
Point 6	0.666	0.686	2.92	1.056	1.080	2.22
Point 7	0.788	0.788	0	1.099	1.102	0.27
Point 8	0.731	0.733	0.27	1.063	1.058	0.47
Average error			0.94			

4.3. Floor Vibration Control Simulation

Since the floor slab exhibited vibration comfort levels below the required standards in several test areas, a simulation was conducted to assess the improvement in vibration comfort following the installation of Tuned Mass Dampers (TMDs).

A Tuned Mass Damper (TMD) is a device used to reduce vibrations in structures. It consists of a mass mounted on a structure with springs and dampers. The TMD is tuned to the structure's natural frequency, so, when the structure vibrates, the TMD counteracts the motion through its own oscillation. This reduces the amplitude of vibrations by dissipating energy, thereby enhancing stability and comfort in structures, especially under dynamic loads like wind or human movement.

4.3.1. Calculation of TMD Parameters

To calculate the parameters for the Tuned Mass Dampers (TMDs) for implementation in finite element software, two key values are required: the total stiffness of the TMD spring and the damping coefficient of the damper. These values can be determined using the following formula:

$$\omega = 2\pi f$$
$$\omega = \sqrt{\frac{k}{m}}$$

The following can be concluded:

$$k = m\omega^2$$

According to the following formula,

$$\xi = \frac{c}{2m\omega}$$

The following can be concluded:

$$c = 2m\omega\xi$$

Given the formulae and the approach discussed earlier for calculating the parameters of Tuned Mass Dampers (TMDs), these calculated parameters would then be summarized in Table 12.

Table 12. TMD finite element calculation parameter table.

Number	k (kN/m)	c (kN·s/m)
TMD1	190,920	1563
TMD2	226,845	1704
TMD3	291,067	1930
TMD4	209,780	1639
TMD5	236,310	1739
TMD6	280,551	1895
TMD7	195,862	1583
TMD8	228,185	1709

4.3.2. TMD Plan Layout and Parameters

The layout plan for the Tuned Mass Dampers (TMDs) is presented in Figure 10, and the specific parameters of the TMDs are provided in Table 13.

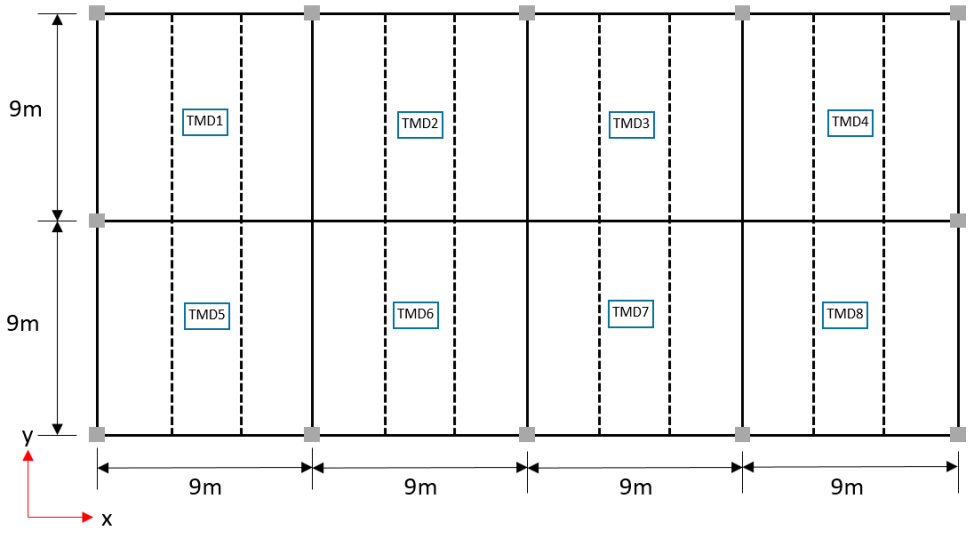


Figure 10. TMD plan layout diagram.

Table 13. TMD parameter table.

Number	m (kg)	f (Hz)	ξ	Maximum Stroke (mm)
TMD1	500	3.11	0.08	±30
TMD2	500	3.39	0.08	±30
TMD3	500	3.84	0.08	±30
TMD4	500	3.26	0.08	±30
TMD5	500	3.46	0.08	±30
TMD6	500	3.77	0.08	±30
TMD7	500	3.15	0.08	±30
TMD8	500	3.40	0.08	±30

4.3.3. Inputting TMD Parameters into Finite Element Software

In finite element software, Tuned Mass Dampers (TMDs) are implemented through the boundary module, specifically within the sub-module for general connection properties. For instance, the parameters for TMD1, as determined from the calculations, are configured as shown in Figure 11. To avoid errors during the simulation process, a relatively small value is assigned to the rotational stiffness due to the software's requirements. The same method is applied to configure the settings for the other TMDs.

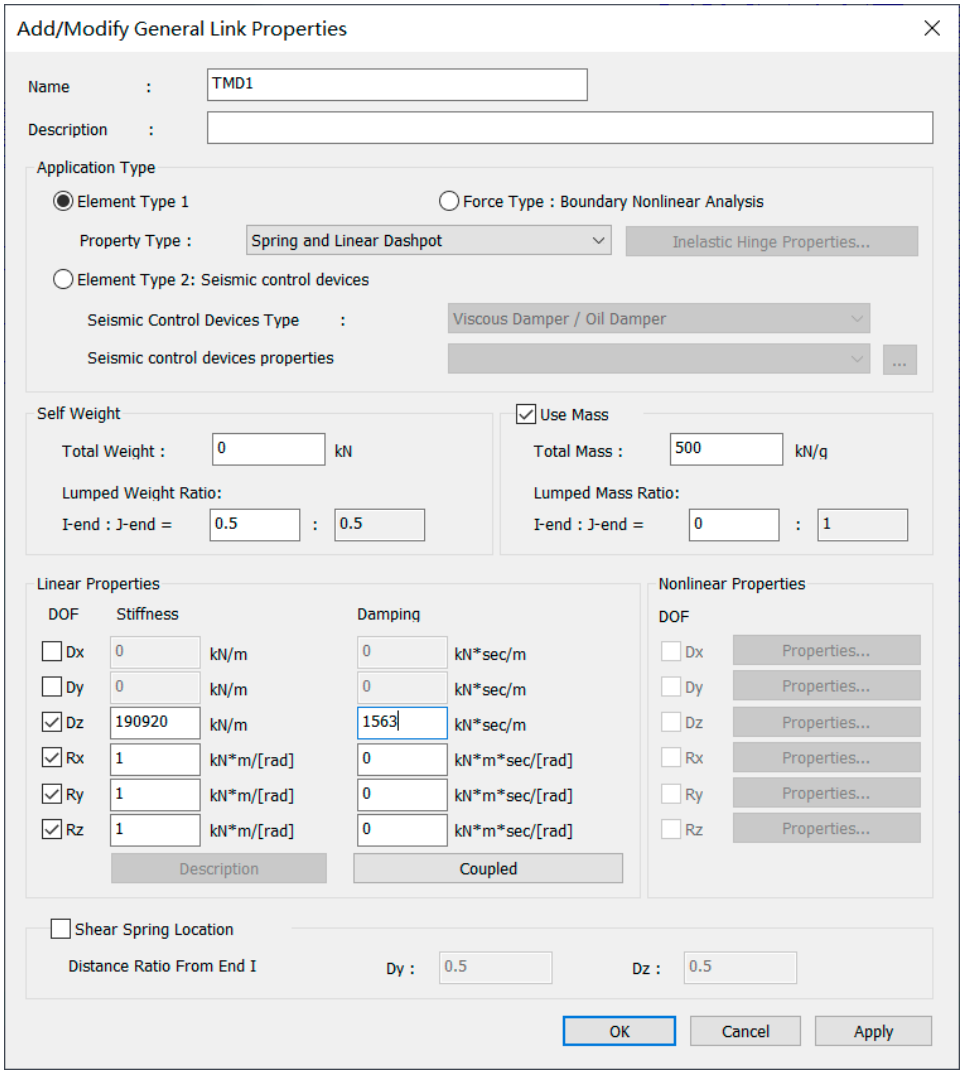


Figure 11. TMD parameter configuration diagram.

4.3.4. Comparison of Vertical Peak Acceleration Before and After TMD Installation

Given that the response to running excitation was the largest among the three conditions tested, the comparison of vertical peak accelerations at measurement points before and after the installation of Tuned Mass Dampers (TMDs) was conducted under running excitation. This comparison is illustrated in Figure 12, and the detailed data are compiled in Table 14.

Table 14. Before and after TMD installation result of peak vertical vibration acceleration.

Measurement Points	Peak Acceleration ($m \cdot s^{-2}$)		Vibration Damping Effect (%)
	Before TMD Installation	After TMD Installation	
1	1.089	0.371	65.93
2	1.265	0.392	69.01
3	0.753	0.261	65.34
4	0.998	0.354	64.53
5	0.720	0.246	65.83
6	1.056	0.371	64.87
7	1.099	0.369	66.42
8	1.063	0.384	63.88
	Average value		65.73

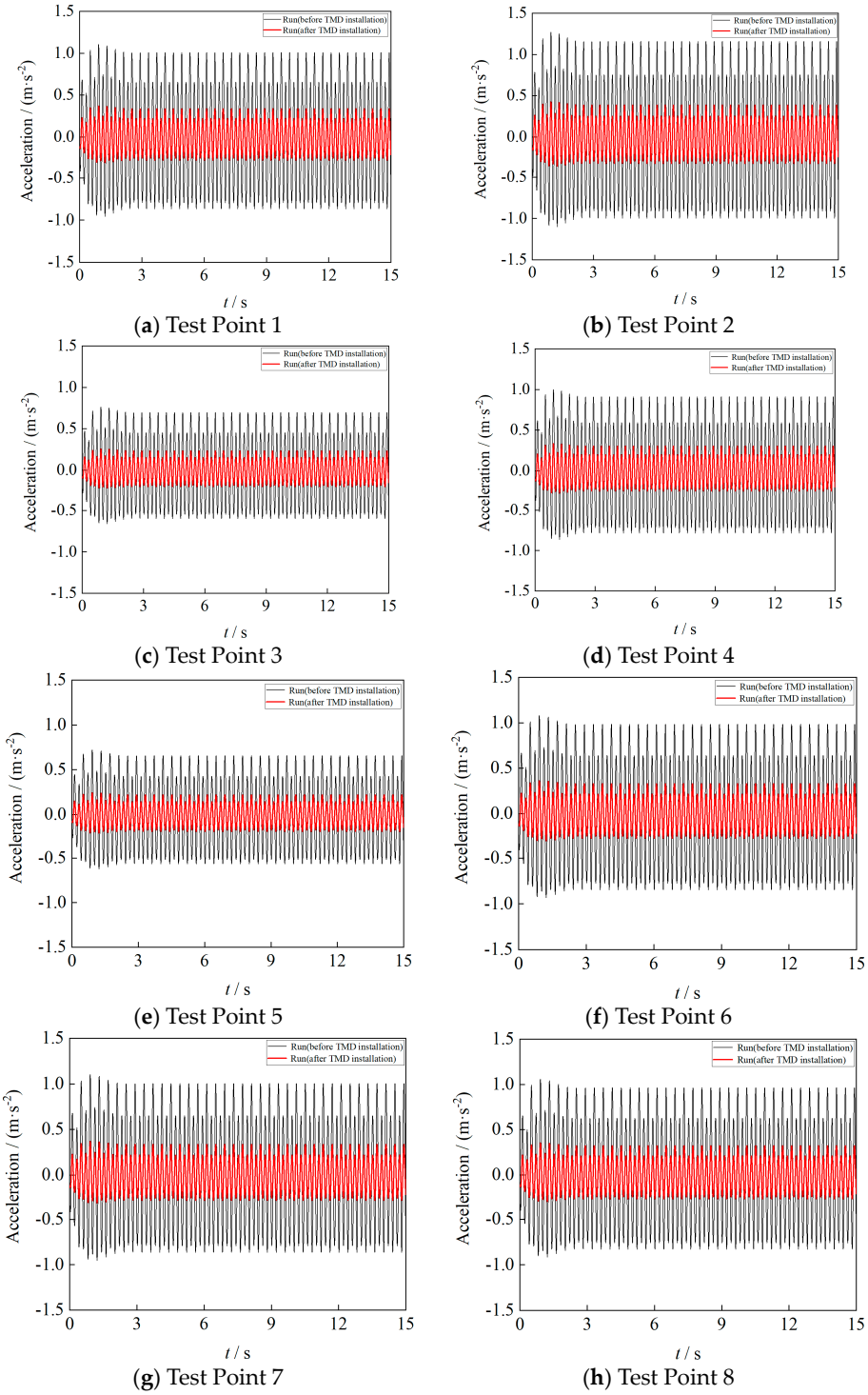


Figure 12. Before and after TMD installation result of time-history curve of vibration acceleration.

As shown in Figure 12 and Table 14, the installation of Tuned Mass Dampers (TMDs) resulted in a significant reduction in vertical peak acceleration across all measurement points, with an average decrease of 65.73%. Furthermore, all measurement points now meet the standard requirement, remaining below the specified limit of 0.4 m·s^{-2}.

5. Conclusions

(1) Floor's Vertical Vibration Comfort Compliance: The steel–concrete composite floor does not meet the vibration comfort standards under human-induced load conditions.

(2) Effectiveness of TMD Installation: The installation of specifically designed Tuned Mass Dampers (TMDs) in vibration-sensitive areas significantly reduced the vibrational response, enabling the steel–concrete composite floor to conform to the floor's vertical vibration comfort standards. After installing the TMD, 100% of the measurement points meet the vibration comfort standards.

Author Contributions: Conceptualization, X.Z. (Xinxin Zhang) and X.Z. (Xiaoxiong Zha); methodology, R.Z.; software, R.Z.; validation, Y.L.; formal analysis, R.Z.; investigation, R.Z. and Y.L.; resources, X.Z. (Xinxin Zhang) and X.Z. (Xiaoxiong Zha); data curation, R.Z.; writing—original draft preparation, R.Z.; writing—review and editing, R.Z.; visualization, R.Z.; supervision, X.Z. (Xinxin Zhang) and X.Z. (Xiaoxiong Zha); project administration, X.Z. (Xinxin Zhang) and X.Z. (Xiaoxiong Zha); funding acquisition, X.Z. (Xinxin Zhang) and X.Z. (Xiaoxiong Zha). All authors have read and agreed to the published version of the manuscript.

Funding: This work supported by the Natural Science Foundation of China (No. 52178129), Science and Technology Planning Project of Shenzhen Municipality (GJHZ20220913143007013), and Science and Technology Planning Project of Shenzhen Municipality (KCXST20221021111408021).

Data Availability Statement: The raw data supporting the conclusions of this article will be made available by the authors on request.

Conflicts of Interest: Authors Xinxin Zhang and Yong Liao are employed by the China Construction Science and Industry Corporation Ltd. The remaining authors declare that the research was conducted in the absence of any commercial or financial relationships that could be construed as a potential conflict of interest.

References

1. Mello, A.D.A.; Da Silva, J.G.S.; Vellasco, P.D.S.; De Andrade, S.A.L.; De Lima, L.R.O. Dynamic analysis of composite systems made of concrete slabs and steel beams. *J. Constr. Steel Res.* **2008**, *64*, 1142–1151. [CrossRef]
2. Kim, S.H.; Cho, K.I.; Choi, M.S.; Lim, J.Y. Development of human body model for the dynamic analysis of footbriges under pedestrian induced excitation. *Steel Struct.* **2008**, *8*, 333–345.
3. Silva, S.; Thambiratnam, D. Dynamic characteristics of steel-deck composite floos under human-induced loads. *Comput. Struct.* **2009**, *87*, 1067–1076. [CrossRef]
4. Song, Z.; Jin, W. Maximum acceleration response spectrum method for long-span floor vibration under walking excitation. *J. Build. Struct.* **2004**, *25*, 57–63. [CrossRef]
5. Chen, Y. Vibration Research and Shock Absorption Research on Long-Span Pedestrian Bridges Under Walking Load Excitation. Master's Thesis, Tsinghua University, Beijing, China, 2007.
6. Chen, X.; Li, A.; Zhang, Z. Vibration reduction design and analysis of long-span floor of large railway station under random crowd load. *J. Southeast Univ. (Nat. Sci. Ed.)* **2010**, *40*, 543–547. [CrossRef]
7. Huang, J.; Lou, Y.; Wang, Q. Comfortable Degree Design for Floor Systems of Health Clubs and Multistory Sports Gymnasium. *Build. Struct.* **2008**, *38*, 102–105. [CrossRef]
8. Li, Q.; Fan, J.; Nie, J. Research on random vibration of large-span buildings under the rhythmic movement of crowds. *Vib. Shock.* **2012**, *31*, 9–15. [CrossRef]
9. Davis, B.; Liu, D.; Murray, T.M. Simplified experimental evaluation of floors subject to walking-induced vibration. *J. Perform. Constr. Facil. ASCE* **2014**, *28*, 04014023. [CrossRef]
10. Zhou, X.; Li, J.; Liu, J.; Cao, L. Study on vibration serviceability of pre-stressed cable RC truss floor system. *Build. Struct.* **2016**, *46*, 1–10. [CrossRef]
11. Liu, J.; Zheng, X.; Li, J. Vibration serviceability of composite slab with prefabricated concrete straight ribbed panels. *J. Build. Struct.* **2019**, *40*, 41–46. [CrossRef]
12. Domizio, M.; Garrido, H.; Ambrosini, D. Single and multiple TMD optimization to control seismic response of nonlinear structures. *Eng. Struct.* **2022**, *252*, 113667. [CrossRef]
13. Caicedo, D.; Lara-Valencia, L.; Blandon, J.; Graciano, C. Seismic response of high-rise buildings through metaheuristic-based optimization using tuned mass dampers and tuned mass dampers inerter. *J. Build. Eng.* **2021**, *34*, 101927. [CrossRef]
14. *JGJ/T 441-2019*; Technical Standard for Vibration Comfort of Building Floor Structures. China Architecture & Building Press: Beijing, China, 2019.

Disclaimer/Publisher's Note: The statements, opinions and data contained in all publications are solely those of the individual author(s) and contributor(s) and not of MDPI and/or the editor(s). MDPI and/or the editor(s) disclaim responsibility for any injury to people or property resulting from any ideas, methods, instructions or products referred to in the content.